

NUMERICAL STUDIES ON FORWARD AND INVERSE SCATTERING ANALYSIS OF LOVE WAVES BY CAVITIES ON INTERFACE

Bin Wang¹⁾, Chen Yang¹⁾, Zhenghua Qian¹⁾ and Sohichi Hirose²⁾

1) College of Aerospace Engineering, Nanjing University of Aeronautics and Astronautics (〒210016, 29 Yudao Jie, Nanjing, China, E-mail: wangbin1982@nuaa.edu.cn)

2) Dept. of Civil Engineering, Tokyo Institute of Technology (〒152-8552, 2-12-1 O-okayama, Meguro-ku, Tokyo, Japan, E-mail: hirose.s.aa@m.titech.ac.jp)

Love waves have great potential in engineering, such as geological inspection and ultrasonic non-destructive testing for near-surface characteristics. A thorough and effective utilization of the Love wave scattering is required. This paper deals with the Love wave scattering by cavity-like flaws located on the layer interface in both forward and inverse aspects. We firstly suggest a numerical approach employing method of fundamental solutions (MFS) and modified boundary element method (BEM) incorporating far-field displacement patterns, which effectively reduces the spurious reflections due to model truncation. We also propose here a quantitative reconstruction procedure for the flaw shape using reflection coefficients of the first order Love wave. By theoretical deduction, it can be proved that the cavity's geometric shape is approximately expressed as an inverse spatial Fourier transform of far-field reflection coefficients in the wavenumber domain. Numerical examples are given and high consistency is shown between the reconstructed flaw images and the geometric characteristics of the actual flaws.

Key Words: Love Wave, Cavity, Boundary Element Method, Method of Fundamental Solutions, Inverse Problem.

1. Introduction

The surface waves, such as Rayleigh and Love waves, are well suited for geological inspection and ultrasonic non-destructive testing, especially for detection of near-surface underground characteristics, such as low-velocity weaknesses, cracks, cavities and delaminations.

Geological engineers have developed various technologies to apply surface waves for reconstruction of underground inhomogeneities, such as reverse time migration (RTM)⁽¹⁾⁽²⁾, surface wave interferometry⁽³⁾, and full waveform inversion (FWI)⁽⁴⁾. The surface waves also have great potential in inspection of large-scale structural members, such as concrete or steel-concrete composite beams and columns. However, in the field of non-destructive testing (NDT), reports on quantitative techniques using surface waves are still few and scattered.

In order to study the interaction between Love surface waves and near-surface flaw, the scattering problem should be solved by numerical approaches. However, the traditional FEM or finite difference

methods are either time-and-memory consuming or difficult to apply complicated boundary conditions.

The boundary element method (BEM) can be an efficient numerical method for solving wave scattering problem since it only requires mesh on boundaries. Due to model truncation, spurious reflection waves may occur at the artificial boundaries⁽⁵⁾. We propose here a modified BEM approach to solve Love wave scattering problems, in which far-field displacement patterns with unknown coefficients were introduced onto the far-field boundaries which have been omitted in traditional BEM configurations⁽⁶⁾. Moreover, the modified BEM are incorporated with method of fundamental solutions (MFS)⁽⁷⁾, in which the flaw areas are characterized by a series of source points with undetermined strengths, which are then substituted into BEM formulation and solved by traction free boundary conditions on the flaw boundaries. The combined MFS-modified BEM approach makes model renew easily realized by only adjusting source positions and local boundary conditions, instead of remeshing the whole model. This

feature is especially useful in iterative inverse reconstruction process.

Moreover, we also propose here a simple inversion procedure to reconstruct cavities on the interface. The inversion method makes use of the reflection coefficients obtained from previous forward analysis as the input data, and reconstruct the vertical flow width in space domain by performing an inverse Fourier transform from these coefficients in wavenumber domain using Born approximation. The reconstruction images of the cavities can not only tell the positions but also the shapes and severity of flaws, and can be used as an initial solution for following iterative reconstruction algorithm.

2. Problem configuration

The problem is defined as shown by Fig. 1. A cavity-like flaw is cut on the interface between the upper layer and lower half-plane. As shown by Fig. 1, symbols $S_1 \sim S_4$ represent the undamaged boundaries in the near-field, whereas $S_{I,II}^{\pm\infty}$ denote their extensions to far-field. $S_5 \sim S_8$ are cavity boundaries, and $S_9 \sim S_{10}$ are intersections of left and right quarter-planes. The vector \mathbf{n} denotes the unit normal direction of boundaries.

An incident wave of a single Love mode is propagating from left to right and interact with the flaw, and the reflected wave generated is observed at the far-field on the left side. We are concerned with the scattering problem and mode conversion of the Love waves.

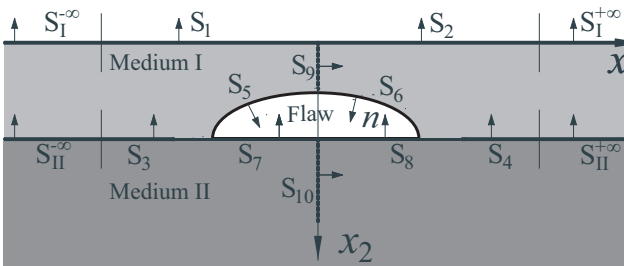


Fig. 1 Problem configuration

3. BEM formulation

The basic BEM formulation for the scattered wave field is shown by Eqs. (1a) and (1b) for the upper and lower media, respectively.

$$\int_{S_1 \cup S_2 \cup S_1^{\pm\infty}} -T_I(\mathbf{x}, \mathbf{X}) u^{\text{sca}}(\mathbf{x}) dS(\mathbf{x}) + \int_{S_3 \cup S_4 \cup S_{II}^{\pm\infty}} (-t^{\text{sca}}(\mathbf{x}) G_I(\mathbf{x}, \mathbf{X}) + T_I(\mathbf{x}, \mathbf{X}) u^{\text{sca}}(\mathbf{x})) dS(\mathbf{x}) \quad (1a)$$

$$\int_{S_5 \cup S_6} (t^{\text{sca}}(\mathbf{x}) G_I(\mathbf{x}, \mathbf{X}) - T_I(\mathbf{x}, \mathbf{X}) u^{\text{sca}}(\mathbf{x})) dS(\mathbf{x}) = C(\mathbf{X}) u^{\text{sca}}(\mathbf{X})$$

$$\int_{S_3 \cup S_4 \cup S_7 \cup S_8 \cup S_{II}^{\pm\infty}} (t^{\text{sca}}(\mathbf{x}) G_{II}(\mathbf{x}, \mathbf{X}) - T_{II}(\mathbf{x}, \mathbf{X}) u^{\text{sca}}(\mathbf{x})) dS(\mathbf{x}) = C(\mathbf{X}) u^{\text{sca}}(\mathbf{X}) \quad (1b)$$

where points \mathbf{x} and \mathbf{X} represent the field and source points, respectively. For the BEM application, both the field and source points are located on the boundaries. The coefficient C takes value of 1/2 as \mathbf{X} is on smooth boundaries, and 1 or 0 as \mathbf{X} locates inside or outside domain considered. G_I and G_{II} are full-plane displacement Green's functions in the upper and lower media, respectively; while T_I and T_{II} are corresponding traction Green's functions. u^{sca} and t^{sca} are the displacement and traction of the scattered wave field, respectively. For the current anti-plane problem, both u^{sca} and t^{sca} are in the x_3 direction, thus the subscript is omitted in the following context. $t^{\text{sca}} = \sigma_{3\alpha}^{\text{sca}} n_\alpha$, in which the normal vectors point upward on the upper surface and the interface, and inward on the flaw boundaries, as shown by small arrows on the boundaries in Fig. 1.

Meanwhile, the fundamental solutions used in BEM formulation is expressed as:

$$G_\alpha(\mathbf{x}, \mathbf{X}) = \frac{i}{4\mu_\alpha} H_0^{(1)}(k_\alpha |\mathbf{x} - \mathbf{X}|), \quad (\alpha = I, II) \quad (2)$$

where $H_0^{(1)}$ is the first kind Hankel function of zeroth order. $|\mathbf{x} - \mathbf{X}|$ represents the distance between source and field points. The Green's function for surface traction can be calculated by elastic stress-strain relations. μ_α and k_α ($\alpha = I, II$) are shear modulus and SH wavenumbers in upper and lower media respectively. Also, $k_\alpha = \omega/c_{T\alpha}$ is the ratio of circular frequency over shear wave velocity.

It is assumed, in the far field, the wave fields are composed of only a series of propagating Love modes, as shown by Eqs. (3a) and (3b).

$$u(x_1, x_2) = \sum_i A_{(i)}^\pm \tilde{u}_{(i)}^\pm(x_1, x_2) = \sum_i A_{(i)}^\pm \hat{u}_{(i)}(x_2) e^{\pm i \xi_{(i)} x_1} \quad (3a)$$

$$\hat{u}_{(i)}(x_2) = \begin{cases} (e^{+R_{(i)} H} + e^{-R_{(i)} H}) e^{-R_{(i)}(x_2 - H)} & (x_2 \geq H) \\ e^{+R_{(i)} x_2} + e^{-R_{(i)} x_2} & (0 < x_2 < H) \end{cases} \quad (3b)$$

where $\tilde{u}_{(i)}^\pm$ represents the unit displacement field for the i th Love mode propagating in positive or negative

directions, respectively; and $A_{(i)}^{\pm}$ and $\hat{u}_{(i)}$ are the i th-order-mode's coefficient and vertical wave profile, as expressed by Eq. (3b). $R_{\alpha(i)} = (\xi_{1(i)}^2 - k_{\alpha}^2)^{1/2}$ are vertical wavenumbers, in which $\xi_{1(i)}$ is the i th propagating wavenumber, i.e. solution of dispersion equation:

$$\mu_1 R_1 (e^{+R_1 H} - e^{-R_1 H}) + \mu_{II} R_{II} (e^{+R_1 H} + e^{-R_1 H}) = 0 \quad (4)$$

Substituting Eqs. (3) and (4) into the infinite boundary terms of Eq. (1), we have:

$$\begin{aligned} & \int_{S_1 \cup S_2} -T_I(\mathbf{x}, \mathbf{X}) u^{\text{sca}}(\mathbf{x}) dS(\mathbf{x}) \\ & + \int_{S_3 \cup S_4} (-t^{\text{sca}}(\mathbf{x}) G_I(\mathbf{x}, \mathbf{X}) + T_I(\mathbf{x}, \mathbf{X}) u^{\text{sca}}(\mathbf{x})) dS(\mathbf{x}) \\ & + \int_{S_5 \cup S_6} (t^{\text{sca}}(\mathbf{x}) G_I(\mathbf{x}, \mathbf{X}) - T_I(\mathbf{x}, \mathbf{X}) u^{\text{sca}}(\mathbf{x})) dS(\mathbf{x}) \\ & + \sum_i A_i^+ I_i^+(\mathbf{X}) + \sum_i A_i^- I_i^-(\mathbf{X}) = C(\mathbf{X}) u^{\text{sca}}(\mathbf{X}) \end{aligned} \quad (5a)$$

$$\begin{aligned} & \int_{S_3 \cup S_4 \cup S_7 \cup S_8} (t^{\text{sca}}(\mathbf{x}) G_{II}(\mathbf{x}, \mathbf{X}) - T_{II}(\mathbf{x}, \mathbf{X}) u^{\text{sca}}(\mathbf{x})) dS(\mathbf{x}) \\ & + \sum_i A_i^+ I_i^{\text{II}+}(\mathbf{X}) + \sum_i A_i^- I_i^{\text{II}-}(\mathbf{X}) = C(\mathbf{X}) u^{\text{sca}}(\mathbf{X}) \end{aligned} \quad (5b)$$

The integrals I_i^{\pm} and $I_i^{\text{II}\pm}$ in Eq. (5) are expressed as shown by Eq. (6).

$$I_i^{\pm}(\mathbf{X}) = \int_{S_1^{\pm\infty}} -T_I(\mathbf{x}, \mathbf{X}) \hat{u}_i^{\pm}(\mathbf{x}) dS(\mathbf{x}) + \int_{S_{II}^{\pm\infty}} (-\tilde{t}_i^{\pm}(\mathbf{x}) G_I(\mathbf{x}, \mathbf{X}) + T_I(\mathbf{x}, \mathbf{X}) \hat{u}_i^{\pm}(\mathbf{x})) dS(\mathbf{x}) \quad (6a)$$

$$I_i^{\text{II}\pm}(\mathbf{X}) = \int_{S_{II}^{\pm\infty}} (-\tilde{t}_i^{\pm}(\mathbf{x}) G_{II}(\mathbf{x}, \mathbf{X}) + T_{II}(\mathbf{x}, \mathbf{X}) \hat{u}_i^{\pm}(\mathbf{x})) dS(\mathbf{x}) \quad (6b)$$

In traditional BEM, the infinite boundaries are often omitted. Instead, a small damping is introduced to count reduce spurious reflections⁽⁶⁾, which makes the problem complex. In the modified BEM method, due to the assumption previously made, the contribution of far-field can be incorporated. Since the integral are taken over infinite boundaries, we apply here the reciprocity theorem of elasto-dynamics⁽⁵⁾ to transfer the integrals onto finite boundaries, as expressed as Eqs. (7) and (8). Since only the Love wave mode is considered, the wave field decays quickly in x_2 direction.

$$I_i^-(\mathbf{X}) = C(\mathbf{X}) \tilde{u}_i^-(\mathbf{X}) - \int_{S_1 \cup S_9 \cup S_5} (\tilde{t}_i^-(\mathbf{x}) G_I(\mathbf{x}, \mathbf{X}) - T_I(\mathbf{x}, \mathbf{X}) \tilde{u}_i^-(\mathbf{x})) dS(\mathbf{x}) \quad (7a)$$

$$\begin{aligned} & + \int_{S_3} (\tilde{t}_i^-(\mathbf{x}) G_I(\mathbf{x}, \mathbf{X}) - T_I(\mathbf{x}, \mathbf{X}) \tilde{u}_i^-(\mathbf{x})) dS(\mathbf{x}) \\ I_i^{\text{II}-}(\mathbf{X}) & = C(\mathbf{X}) \tilde{u}_i^-(\mathbf{X}) - \int_{S_3 \cup S_7 \cup S_{10}} (\tilde{t}_i^-(\mathbf{x}) G_{II}(\mathbf{x}, \mathbf{X}) - T_{II}(\mathbf{x}, \mathbf{X}) \tilde{u}_i^-(\mathbf{x})) dS(\mathbf{x}) \end{aligned} \quad (7b)$$

$$I_i^+(\mathbf{X}) = C(\mathbf{X}) \tilde{u}_i^+(\mathbf{X}) - \int_{S_2 \cup S_6} (\tilde{t}_i^+(\mathbf{x}) G_I(\mathbf{x}, \mathbf{X}) - T_I(\mathbf{x}, \mathbf{X}) \tilde{u}_i^+(\mathbf{x})) dS(\mathbf{x}) + \int_{S_9 \cup S_4} (\tilde{t}_i^+(\mathbf{x}) G_I(\mathbf{x}, \mathbf{X}) - T_I(\mathbf{x}, \mathbf{X}) \tilde{u}_i^+(\mathbf{x})) dS(\mathbf{x}) \quad (8a)$$

$$I_i^{\text{II}+}(\mathbf{X}) = C(\mathbf{X}) \tilde{u}_i^+(\mathbf{X}) - \int_{S_8 \cup S_4} (\tilde{t}_i^+(\mathbf{x}) G_{II}(\mathbf{x}, \mathbf{X}) - T_{II}(\mathbf{x}, \mathbf{X}) \tilde{u}_i^+(\mathbf{x})) dS(\mathbf{x}) + \int_{S_{10}} (\tilde{t}_i^+(\mathbf{x}) G_{II}(\mathbf{x}, \mathbf{X}) - T_{II}(\mathbf{x}, \mathbf{X}) \tilde{u}_i^+(\mathbf{x})) dS(\mathbf{x}) \quad (8b)$$

4. Combination of BEM and MFS

In order to increase the calculation efficiency, we propose here a method combining modified BEM with method of fundamental solution (MFS), which assumes the defect has the same effect with a series of point sources in forming the scattered wave. The artificial point sources are located in the interior domain of the cavity near the surface, as shown by Fig. 2. The strengths of the sources are determined by imposing free-traction conditions on the collocation points on the cavity boundaries.

Then, the boundary integral equation of the upper layer is rewritten by the following means:

$$\begin{aligned} & \int_{S_1 \cup S_2} -T_I(\mathbf{x}, \mathbf{X}) u^{\text{sca}}(\mathbf{x}) dS(\mathbf{x}) + \int_{S_3 \cup S_4} (-t^{\text{sca}}(\mathbf{x}) G_I(\mathbf{x}, \mathbf{X}) + T_I(\mathbf{x}, \mathbf{X}) u^{\text{sca}}(\mathbf{x})) dS(\mathbf{x}) \\ & + \sum_i A_i^+ I_i^+(\mathbf{X}) + \sum_i A_i^- I_i^-(\mathbf{X}) + \sum_k B_k G(s_k, \mathbf{X}) \\ & = C(\mathbf{X}) u^{\text{sca}}(\mathbf{X}) \end{aligned} \quad (9)$$

where s_k is the location of the k th source, B_k is its strength.

Since the cavity boundaries are no longer explicit in the BEM formation, the boundaries S_7 and S_8 have been merged into nearby S_3 and S_4 , respectively; while the virtual boundary S_9 is extended to meet the interface of upper layer and half-plane.

The BIE for the lower half-plane keeps the same form with Eq. (5b), with only the notations for integral boundaries $S_3 \cup S_4 \cup S_7 \cup S_8$ in Fig. 1 replaced with

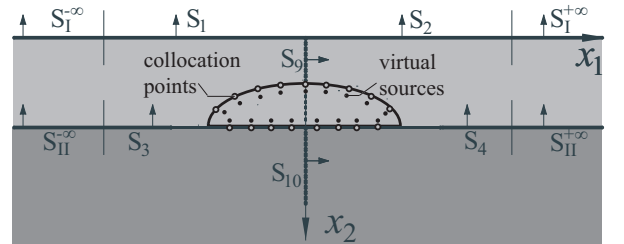


Fig. 2 Configuration of MFS

$S_3 \cup S_4$ in Fig. 2, since no source is set in the half-plane. Additional parameters B_k are solved by imposing free-traction conditions on collocation points on flaw boundaries.

By combining Eqs. (7) and (9), the unknown parameters A_i^\pm and B_k are solved, together with displacements and tractions on boundaries $S_1 \cup S_2$ and interfaces $S_3 \cup S_4$.

5. Numerical examples for forward problem

A two-dimensional artificial cavity of circular-segment shape is cut from the upper-layer material on the interface. As shown by Fig. 3, the thickness of upper layer is H , and the cavity's arc radius is R , the maximum vertical height h . The shear modulus and density of the lower half-plane and the upper layer is μ_{II} , ρ_{II} , μ and ρ , respectively. The physical parameters are kept same as the previous example; and the arc radius R is set equal to the upper layer thickness H (i.e. $R/H=1.0$), while the cavity's vertical depth is $h/H=0.2$.

The incident wave is a unit fundamental (first) Love mode:

$$u^{\text{inc}}(x_1, x_2) = \hat{u}_{(1)}(x_2) e^{+i\xi_{(1)}x_1} \quad (10)$$

For which the reflected wave field at far fields are:

$$u^{\text{ref}}(x_1, x_2) = \sum_i \text{Coe}_{(i)} \hat{u}_{(i)}(x_2) e^{-i\xi_{(i)}x_1} \quad (11)$$

where $\text{Coe}_{(i)}$ is the reflection coefficient for the i th mode, in which we are especially concerned with that of the first mode $\text{Coe}_{(1)}$. By applying the modified BEM approach, we are able to obtain the steady-state displacements and tractions of the scattered wave for the near-field and the reflection coefficients for far-fields at various frequencies, as shown by Fig. 4.

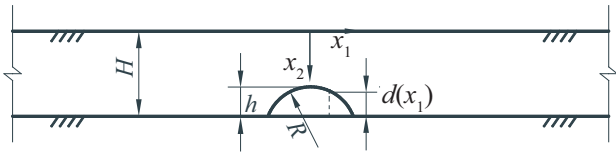


Fig. 3 Geometric parameters of numerical examples

6. Inverse problem

The aim of the inverse problem is to reconstruct the location and shape of cavity on the interface from reflection coefficients obtained previously.

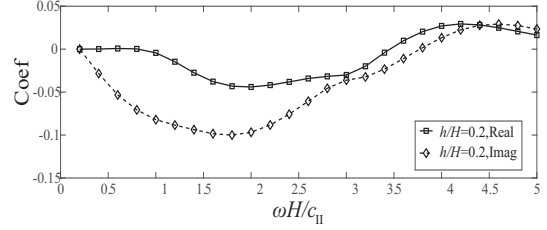


Fig. 4 Reflection coefficients

Mathematically, the objective function is the vertical depth $d(x_1)$ over the horizontal coordinate. The function value reduces to zero at intact parts. The reflection coefficients of the first mode, i.e. $\text{Coe}_{(1)}$ is used here.

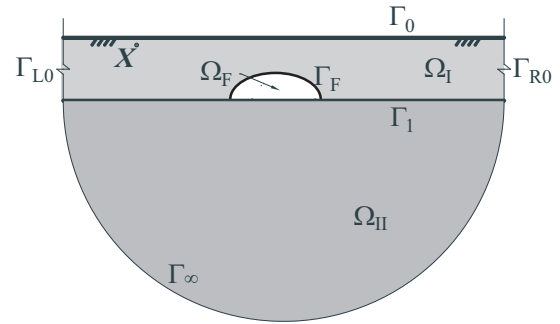


Fig. 5 Inverse problem configuration

The configuration of inverse problem is illustrated by Fig. 5, where the upper surface, layer interface and the flaw surface are termed as Γ_0 , Γ_1 and Γ_F , respectively; and the outer boundaries Γ_{L0} , Γ_{R0} and Γ_∞ tend toward infinity. The bounded domains in the upper layer, the lower half plane and the cavity interior are Ω_I , Ω_{II} and Ω_F , respectively. The observation point is X .

For the derivation of inversion, we introduce here the Green's functions⁽⁸⁾ for the layered half-plane G^h and T^h . For simplicity, in following deduction we no longer distinguish the expressions of G^h and T^h in different materials. But the readers should bear in mind that they take different material parameters for different layers.

We write the boundary integral equation (BIE) of the incident wave field for finite volume Ω_F , with source of Green's function put at point X , where the normal vector of the boundary Γ_F pointing inward.

$$\int_{\Gamma_F} (-t^{\text{inc}}(x) G^h(x, X) + T^h(x, X) u^{\text{inc}}(x)) dS = 0 \quad (12)$$

Similarly, we can write the BIE of the scattered wave for the infinite region $\Omega_I \cup \Omega_{II} \cup \overline{\Omega_F}$, with source point of Green's function also at \mathbf{X} ,

$$\int_{\Gamma_0 \cup \Gamma_{L0} \cup \Gamma_{R0} \cup \Gamma_\infty \cup \Gamma_F} (t^{\text{sca}}(\mathbf{x}, \mathbf{X}) G^{\text{h}}(\mathbf{x}, \mathbf{X}) - T^{\text{h}}(\mathbf{x}, \mathbf{X}) u^{\text{sca}}(\mathbf{x})) dS(\mathbf{x}) = u^{\text{sca}}(\mathbf{X}) \quad (13)$$

in which the normal vector on the outer boundaries are pointing outward.

Subtracting Eq. (13) with (12), we can now write the boundary integral equations (BIE) for the scattered wave at point \mathbf{X} . by relation $u^{\text{tot}} = u^{\text{inc}} + u^{\text{sca}}$, we have:

$$\int_{\Gamma_0 \cup \Gamma_{L0} \cup \Gamma_{R0} \cup \Gamma_\infty} (t^{\text{sca}}(\mathbf{x}, \mathbf{X}) G^{\text{h}}(\mathbf{x}, \mathbf{X}) - T^{\text{h}}(\mathbf{x}, \mathbf{X}) u^{\text{sca}}(\mathbf{x})) dS(\mathbf{x}) + \int_{\Gamma_F} (t^{\text{tot}}(\mathbf{x}, \mathbf{X}) G^{\text{h}}(\mathbf{x}, \mathbf{X}) - T^{\text{h}}(\mathbf{x}, \mathbf{X}) u^{\text{tot}}(\mathbf{x})) dS(\mathbf{x}) = u^{\text{sca}}(\mathbf{X}) \quad (14)$$

The integral of $t^{\text{sca}} G^{\text{h}} - T^{\text{h}} u^{\text{sca}}$ over boundaries toward infinity $\Gamma_{L0} \cup \Gamma_{R0} \cup \Gamma_\infty$ vanishes due to radiation conditions⁽⁹⁾, so do the one on surface Γ_0 due to free traction t^{sca} and T^{h} . The integral of $t^{\text{tot}} G^{\text{h}}$ also vanishes on Γ_F due to free traction t^{tot} on the flaw boundary. Thus, Eq. (14) becomes:

$$-\int_{\Gamma_F} \mu_1 n_\alpha G_{,\alpha}^{\text{h}}(\mathbf{x}, \mathbf{X}) u^{\text{tot}}(\mathbf{x}) dS(\mathbf{x}) = u^{\text{sca}}(\mathbf{X}) \quad (15)$$

where we have expressed $T^{\text{h}}(\mathbf{x}, \mathbf{X})$ by $G^{\text{h}}(\mathbf{x}, \mathbf{X})$ through stress-displacement relation. As the cavity is small, we can apply Born approximation to Eq. (15), replacing u^{tot} with u^{inc}

Since Γ_F is closed, we can transfer the boundary integral into volume integral by Gauss's theorem:

$$-\mu_1 \int_{\Omega_F} \left[-k_1^2 G^{\text{h}}(\mathbf{x}, \mathbf{X}) u^{\text{inc}}(\mathbf{x}) + G_{,\alpha}^{\text{h}}(\mathbf{x}, \mathbf{X}) u_{,\alpha}^{\text{inc}}(\mathbf{x}) \right] dV = u^{\text{sca}}(\mathbf{X}) \quad (16)$$

Then the expressions of incident wave, and the Green's functions are substituted into Eq. (16):

$$u^{\text{sca}}(\mathbf{X}) = -2i\mu_1 f(\xi_1) \times \int_{\Omega_F} \left(k_1^2 (e^{+2R_1 x_2} + e^{-2R_1 x_2}) + 2\xi_1^2 \right) e^{+2i\xi_1 x_1} dV(\mathbf{x}) \times (e^{+R_1 X_2} + e^{-R_1 X_2}) e^{-i\xi_1 X_1} \quad (17)$$

where $f(\xi_1)$ is defined as:

$$f(\xi_1) = \frac{e^{+R_1 H}}{L'(\xi_1)(1 + e^{+2R_1 H})} \quad (18a)$$

$$L(\xi_1) = \mu_1 R_1 (e^{+R_1 H} - e^{-R_1 H}) + \mu_{II} R_{II} (e^{+R_1 H} + e^{-R_1 H}) \quad (18b)$$

Rewrite the volume integral into dual integral:

$$\int_{\Omega_F} dV(\mathbf{x}) \rightarrow \int_{-\infty}^{\infty} \int_{H-d(x_1)}^H dx_2 dx_1$$

Here the vertical width of cavity $d(x_1)$ is our objective function. The value of d takes 0 at intact parts.

Performing Taylor expansion with respect of x_2 at $d(x_1) = 0$, and omitting all the higher-order terms than 0, we have finally:

$$d(x_1) = \int_{-\infty}^{\infty} \frac{C^{\text{ref}}(\xi_1)}{-2i\mu_1 f(\xi_1)(k_1^2(e^{+2R_1 H} + e^{-2R_1 H}) + 2\xi_1^2) \times e^{-2i\xi_1 x_1} d(2\xi_1)} d\xi_1 \quad (19)$$

where $C^{\text{ref}}(\xi_1)$ is the reflection coefficients of the incident mode, expressed in wavenumber domain.

By Eq. (19) we can obtain the objective function $d(x_1)$ on the whole x_1 axis, hence, the position and shape of flaw are reconstructed.

7. Numerical examples for inverse problem

We still use the configuration of Fig. 3 as the numerical example for the inverse problem. Our aim is to reconstruct the vertical width of the cavity over coordinate x_1 .

We make use of the reflection coefficients of the first order i.e. fundamental Love wave impinged on an arc-shaped cavity model with depth $h/H = 0.2$, which have been obtained numerically from modified BEM (see Fig. 4) as the input data for the inversion process. It should be noted, in practice, the reflection coefficients can also be obtained from experiments by performing temporal and spatial Fourier transforms to the received reflected wave signals.

The inversion results are shown as Fig. 6, in which the bold curves represent the results of inverse reconstruction, while the thin ones are the actual flaw shapes. Generally, the reconstructed images agree with the actual flaw shapes in terms of depth, widths and shapes.

From the illustrated and other examples, we can find that, as the cavity is shallow compared with the thickness of the upper layer, its reconstructed image can match the actual shape to a great extent. As the cavity becomes bigger, the reconstructed result becomes coarser. However, its approximate width and depth can still be estimated with enough accuracy.

This inverse reconstruction approach differs from traditional ultrasonic pitch-catch or time-of-flight methods in that it makes use of reflection data of multiple frequency components. The lower frequency components give the location and width of the cavity,

while higher frequency components reconstruct the detailed shape ⁽¹⁰⁾.

8. Conclusion

Our research proposes an effective forward and inverse numerical method for near-surface cavities by means of guided Love surface waves, since the original flaw shape can be reconstructed to a great extent, by means of the inversion technique and the reflection data of forward analysis. For numerical verifications, we propose a modified BEM approach combined with

method of MFS to calculate reflection coefficients at various frequency points of the incident 1st-order Love wave impinging on the cavity.

As the main aim of the paper, we formulate the inverse reconstruction approach, which makes full use of reflection coefficient data and can obtain a good estimation of the location, shape and severity of the cavity simultaneously. The work provided in the paper can provide as a theoretical reference for quantitative non-destructive testing using guided surface waves.

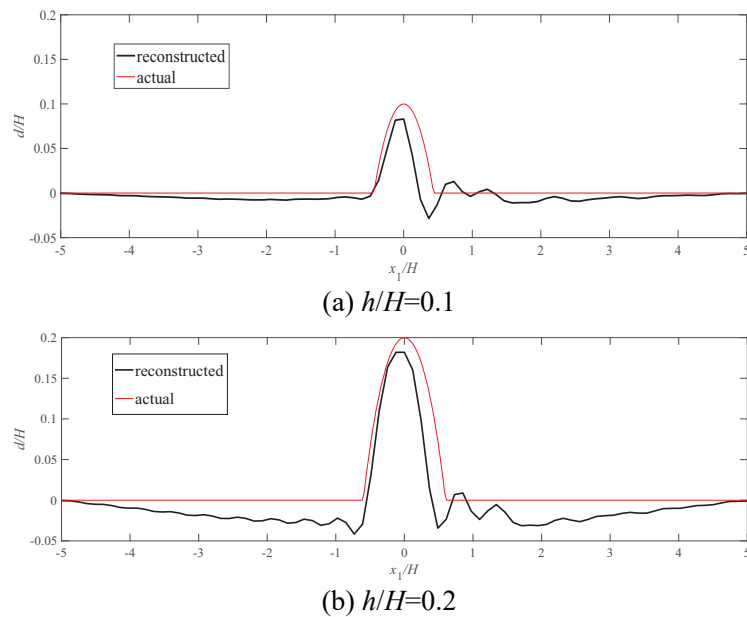


Fig. 6 Reconstructed cavity shapes

References

- (1) A. M. Almuheidib and M. N. Toksoz, Imaging of near-surface heterogeneities by scattered elastic waves, *Geophysics* **80** (2015) A83.
- (2) A. AlTheyab, F. -C. Lin, and G. T. Schuster, Imaging near-surface heterogeneities by natural migration of backscattered surface waves, *Geophys. J. Int.* **204** (2016) 1332.
- (3) A. Kaslilar, U. Harmankaya, K. van Wijk, K. Wapenaar and D. Draganov, Estimating location of scatterers using seismic interferometry of scattered Rayleigh waves, *Near Surface Geophys.* **12** (2014) 721.
- (4) J. Virieux and S. Operto, An overview of full-waveform inversion in exploration geophysics. *Geophysics* **74** (2009) WCC1.
- (5) I. Arias and J. D. Achenbach, Rayleigh wave correction for the BEM analysis of two-dimensional elastodynamic problems in a half-plane, *Int. J. Numer. Meth. Engng.*, **60** (2004) 2131.
- (6) J. Domínguez *Boundary Elements in Dynamics*. Computational mechanics publications, Elsevier applied science: Amsterdam, 1993.
- (7) I. Castro and A. Tadeu, Coupling of the BEM with the MFS for the numerical simulation of frequency domain 2-D elastic wave propagation in the presence of elastic inclusions and cracks, *Eng. Anal. Bound. Elem.*, **36** (2012) 169.
- (8) M. Bouchon, A simple method to calculate Green's functions for elastic layered media, *Bull. Seism. Soc. Am.*, **71**(1981) 959.
- (9) A. I. Madyarov and B. B. Guzina, A radiation condition for layered elastic media. *J. Elasticity*, **82** (2006) 73.
- (10) B. Wang and S. Hirose, Inverse problem for shape reconstruction of plate-thinning by guided SH-waves. *Mater. Trans.*, **53** (2012) 1782.